The Control of Flexible-Link Robots Manipulating Large Payloads: Theory and Experiments

• • • • • • • • • • • • • • •   • • • • • • • • • • • • • • •

Eftychios G. Christoforou
Department of Mechanical Engineering
University of Canterbury
Private Bag 4800
Christchurch, New Zealand

Christopher J. Damaren*
University of Toronto
Institute for Aerospace Studies
4925 Dufferin Street
Toronto, Ontario M3H 5T6, Canada
e-mail: cjd@sdr.utias.utoronto.ca

The control problem for flexible-multilink robots carrying large payloads is revisited. A set of nonlinear approximate equations describing the payload-dominated dynamics of the flexible plant is used in conjunction with the passivity property satisfied by a suitably defined modified input–output pair for the system, to derive a globally asymptotically stable controller together with its adaptive counterpart. Experimental results involving a specially designed 3-degree-of-freedom planar arm with two flexible links, demonstrate their ability to combine end-point tracking with simultaneous active suppression of the vibrations. © 2000 John Wiley & Sons, Inc.

1. INTRODUCTION

Robots have been successfully employed in space operations to improve productivity and reduce the cost and risk involved by enhancing astronaut capabilities and performing tasks that would otherwise have to be undertaken by humans.[1] They are capable of performing a variety of tasks such as deploy- ment and retrieval of objects from the Shuttle's cargo bay, the assembly of large space assets, cap- ture and despinning of satellites, and performing various scientific experiments. The simultaneous re- quirements of minimizing launch mass and a large work space yield robots with long lightweight links which are inherently flexible.

A different philosophy prevails in the design of industrial robots, which have traditionally been very heavy and bulky structures so that undesirable flex-

*To whom all correspondence should be addressed.

ibility effects are not encountered. Consequently, for a typical, manipulator operating in an industrial environment, the ability to perform rapid maneuvers is fairly limited, high capacity actuators are required, the cost is high, and the operation is energy inefficient. Lightweight flexible models exhibit many desirable features and have the potential to replace conventional designs in many terrestrial-based applications.

Control of flexible manipulators constitutes an engineering challenge due to the highly nonlinear nature of the problem, which combines the multibody and structural dynamics together with a difficult controller design problem. It belongs to the class of problems with less control inputs than number of degrees-of-freedom (DOF), and also exhibits noncollocation of control inputs and outputs. Flexible-link robots should be seen from the perspective of a more general trend in modern engineering practice: the desire to accomplish demanding performance, economic or other objectives, often results in solutions which are inherently more difficult to control, and control becomes the critical factor for their success. The case of a high performance aircraft identified by Vidyasagar[2] provides a familiar example of this trend. Its stability often has to be achieved by exclusively active means to enjoy higher speed and better maneuverability at certain flying conditions.

Control for rigid robots has traditionally been joint-based: given a desired task-space trajectory the control objective translates to having the joint DOF follow the corresponding joint-space one, which can be obtained through inverse kinematics as a purely geometric solution. In the flexible-link case, it is obvious that such strategies are in general not suitable and something more sophisticated is required which takes into consideration the elastic nature of the plant.

The vast majority of published work on the control of flexible manipulators has concentrated on the one-link case which is adequately modeled as a linear time-invariant (LTI) system. Although most work on flexible arms has been supported by simulation studies, there have been relatively few convincing experimental results, especially in the multi-link case. Our attention in the following survey is restricted to those works presenting experimental results.

The pioneering work of Cannon and Schmitz[3] demonstrated that a model using unconstrained (pinned-free) modes and a well-designed LTI controller based on this model (they used the Linear Quadratic Gaussian (LQG) technique) could be quite successful. Oakley and Cannon[4] experimentally demonstrated that a Linear Quadratic Regulator (LQR) feedback design coupled with the use of an extended Kalman filter for (nonlinear) state estimation could be used to accurately control a two-link arm with one flexible link. Carusone, Buchan, and D'Eleuterio[5] used gain-scheduled LQR state-feedback designs to successfully control a two-link manipulator with very flexible links. The work of Demeo et al.[6] was concerned with the design of active vibration suppression for the Space Shuttle remote manipulator system. They identified multi-input multi-output (MIMO) LTI models using the Observer–Kalman filter identification (OKID) technique which also provided an estimator gain matrix. State feedback was designed by LQR. Of relevance to our work is the outcome of the human-in-the-loop trials wherein all of the astronauts expressed concern about heavy payloads. Robust control methods were used in the follow-up work[7] to evaluate the active damping achieved for heavy and light payloads.

The nonminimum phase nature of the mapping from joint torques to end-effector motion for flexible-link robots leads to noncausal solutions for the inverse dynamics problem and complication of the feedback design problem. Bayo et al.[8] developed a procedure for solving the inverse dynamics problem and experimentally demonstrated its efficacy in the multilink case. The work of Paden et al.[9] developed causal approximations of this feedforward signal and exploited the passivity property of the torque to joint rate map for joint-based feedback design. This approach was used to control the tip motion of a two-link flexible arm without tip measurements.

Adaptive control has been very successful in controlling rigid robots where the passivity property associated with the joint motion has been heavily exploited. The absence of this property with respect to the end-effector motion in the flexible case may explain why little work has been done on the adaptive control of structurally flexible-multi-link robots. In the single-link case, most approaches have identified LTI models (transfer functions) and used this model for controller design.[10]

The seeds for the passivity-based approach used in this article were sown by Wang and Vidyasagar[11,12] who introduced the reflected tip position in the single-link case. Their motivation stemmed from the ill-defined nature of the relative degree of the transfer function involving the true tip position. In the case of the reflected tip position, a

transfer function of relative degree 2 exists independent of the number of modeled modes[11] and the use of a filtered derivative feedback provided good tracking of step-like commands.[12] The passivity property associated with the reflected tip rate was further studied by Pota and Vidyasagar.[13]

The approach employed here for the case of a flexible-link robot carrying a large payload, effectively exploits an approximate form of the payload-dominated dynamics in conjunction with a modified input and output. The input is created by multiplying the joint torques by the inverse transpose of the rigid Jacobian matrix. The output is a multilink generalization of the reflected tip rate and gives rise to a passive input–output (I–O) map. A nonlinear control strategy is developed together with its adaptive companion, which is capable of dealing with parameter uncertainty associated with the robot and payload. Both controllers are supported by proofs that the tracking of the prescribed end-effector motion exhibits global asymptotic stability. Their ability to achieve task-space tracking with simultaneous active vibration suppression is demonstrated with a set of experimental results involving a planar 3-DOF robot with two flexible links.

Given suitable implementation assumptions, the controllers presented here do not require measurement of the elastic coordinates; however, end-effector measurements are required. The solution of the complex inverse dynamics problem for flexible arms is avoided in generating the feedforward. Given their basis in passivity theory they exhibit strong robustness properties assuming the large payload assumption is honored. This is in strong contrast to methods employing LQR state-feedback design.

2. SYSTEM MODELING

The manipulator is modeled as a chain of N flexible and/or rigid bodies $\{\mathbf{B}_0, \mathbf{B}_1, \ldots, \mathbf{B}_N\}$ and a reference frame $\mathbf{F}_n$ is rigidly attached to each one to describe its position and orientation. $\mathbf{B}_0$ is taken to be rigid and fixed, whereas body $\mathbf{B}_{N+1}$ is a rigid payload attached to the tip of the robot in a cantilevered fashion. Its body frame $\mathbf{F}_{N+1}$ locates the end-effector within the operational space. Since our main motivation stems from space applications, gravity effects are not taken into account, and single-DOF rotational joints between bodies are considered.

The assumed-modes method was selected for the discretization of the link deflections and cantilevered shape functions were found to be a suit-

able choice. The elastic deformation in $\mathbf{B}_n$ is represented as $u_n(\mathbf{r}_n, t) = \mathbf{\Psi}_n(\mathbf{r}_n)\mathbf{q}_{n,e}(t)$ with $\mathbf{\Psi}_n$ the row matrix of shape functions, $\mathbf{q}_{n,e}$ the column of the elastic coordinates for $\mathbf{B}_n$, and the vector $\mathbf{r}_n$ denotes position relative to $\mathbf{F}_n$. Using this method, a finite-dimensional model for the system can be obtained, which retains a sufficiently large number of vibration modes and truncates the rest. This approach is well suited to a Lagrangian formulation for determining the equations of motion, which are of the following standard form,

$$M(\mathbf{q})\ddot{\mathbf{q}} + D\dot{\mathbf{q}} + K\mathbf{q} + C(\mathbf{q}, \dot{\mathbf{q}})\dot{\mathbf{q}} = [\mathbf{1}\ \mathbf{O}]^T \boldsymbol{\tau}(t)$$
$$\mathbf{q} \triangleq \mathrm{col}\{\boldsymbol{\theta}, \mathbf{q}_e\} \quad (1)$$

where $\boldsymbol{\theta}$ is the column of joint rotations and $\mathbf{q}_e = \mathrm{col}\{\mathbf{q}_{n,e}\}$. The mass matrix M, the structural damping matrix D, and the stiffness matrix K can be partitioned consistent with the definition of $\mathbf{q}$ as

$$M = \begin{bmatrix} M_{\theta\theta} & M_{\theta e} \\ M_{\theta e}^T & M_{ee} \end{bmatrix} \qquad K = \begin{bmatrix} \mathbf{O} & \mathbf{O} \\ \mathbf{O} & K_{ee} \end{bmatrix}$$

$$D = \begin{bmatrix} \mathbf{O} & \mathbf{O} \\ \mathbf{O} & D_{ee} \end{bmatrix} \quad (2)$$

with $M = M^T > \mathbf{O}$, $K_{ee} = K_{ee}^T > \mathbf{O}$, and $D_{ee} = D_{ee}^T > \mathbf{O}$. The vector $\boldsymbol{\tau}$ is the control input and C is the matrix with the nonlinear centrifugal and Coriolis terms. A symbolic mathematics computer package was found to be a powerful tool in deriving these equations in a closed form, suitable for the simulation of the dynamic behavior of the system and the software implementation of the controllers.

The generalized position of the end effector is described by a vector $\boldsymbol{\rho}$, whose upper part consists of the position coordinates and at the bottom are three Euler angles parametrizing its orientation with respect to the base frame. The velocity of the end effector is related to the generalized coordinate rates by

$$\dot{\boldsymbol{\rho}} = J_\theta(\boldsymbol{\theta}, \mathbf{q}_e)\dot{\boldsymbol{\theta}} + J_e(\boldsymbol{\theta}, \mathbf{q}_e)\dot{\mathbf{q}}_e \quad (3)$$

where J_θ is the rigid Jacobian and J_e the elastic one.[14]

3. THE PASSIVITY PROPERTY AND PAYLOAD-DOMINATED DYNAMICS

The concept of passivity, which was originally used in network theory, has become a fundamental concept in feedback control. A network is defined as

passive if it contains no sources of energy, i.e., it consists of passive R−L−C elements which only dissipate or store energy but no active elements like voltage or current generators. The importance of passivity in control engineering resides in its close relation with stability as expressed by the passivity theorem, which states that the feedback interconnection of a passive system and a strictly passive system with finite gain is L_2-stable, meaning that finite energy inputs yield finite energy outputs.

It is interesting to note that controllers originally derived using more conventional techniques based on Lyapunov's method, were later interpreted in terms of the passivity theory. A classic example is provided by Ortega and Spong[15] where the term *passivity-based-control* was coined. A complete treatment of this elegant approach can be found in Ortega et al.,[16] where various control system design approaches for Euler−Lagrange systems are examined. Some basic definitions from passivity theory[17] necessary for the development to follow are presented here.

A system H with input $u \in L_{2e}$ and output $y = Hu \in L_{2e}$ is *strictly passive* if there exists $\epsilon > 0$ such that:

$$\int_0^T u^T y \, dt \geq \epsilon \int_0^T u^T u \, dt$$
$$\forall u \in L_{2e} \qquad \forall T > 0 \quad (4)$$

If the above is satisfied with $\epsilon = 0$, the system is *passive*.

In the case of rigid robots, it is well known that the mapping from torques to joint rates is passive. This result relies on the collocation of control inputs and outputs and explains why most of the traditional robotic control schemes actually work. In the context of flexible-link robots this property persists but is less strategic for controller design purposes than it is for the rigid case, since the actual objective is the tracking of a prescribed task-space trajectory.

An important case involving flexible robots arises when a large payload is manipulated by the robot, because the deformations are greater and the vibration frequencies of the system drop. Such cases commonly occur in space manipulation scenarios where robots are required to manipulate objects whose mass is much larger than their own. It is sufficient to mention that robots which assist in building the International Space Station are also required to perform the docking of the Space Shuttle to the station.

Given the desirability of the passivity property, Damaren[14] examined the payload-dominated multi-link flexible case and defined the following modified I−O pair:

$$\hat{\boldsymbol{\tau}}(t) \triangleq J_\theta^{-T} \boldsymbol{\tau}$$
$$\dot{\boldsymbol{\rho}}_\mu \triangleq J_\theta \dot{\boldsymbol{\theta}} + \mu J_e \dot{\mathbf{q}}_e = \dot{\boldsymbol{\rho}} - (1 - \mu) J_e(\boldsymbol{\theta}, \mathbf{q}_e) \dot{\mathbf{q}}_e \quad (5)$$

For the duration of the article, it is assumed that kinematically singular configurations are not encountered. The modified output $\dot{\boldsymbol{\rho}}_\mu$ is called the μ-tip rate, where μ is a real parameter. The true tip rates are captured by $\mu = 1$ while $\mu = 0$ considers only joint-induced motion. It was shown that the mapping from $\hat{\boldsymbol{\tau}}$ to $\dot{\boldsymbol{\rho}}_\mu$ is passive for $\mu < 1$ when large payloads are involved. For $\mu = 1$ the mapping remains passive but the vibration modes become unobservable from the tip rates. It is important to note that $\dot{\boldsymbol{\rho}}_\mu$ provides an effective way to introduce the elastic motion into the control input of a suitable feedback controller and add damping to the vibration modes. For $\mu = -1$, $\dot{\boldsymbol{\rho}}_\mu$ defines the multilink generalization of the reflected tip rate.

A derivation of an approximate (nonlinear) form of the dynamics governing a structurally flexible manipulator carrying a massive payload was presented by Damaren.[18] The equations were derived using a Lagrangian approach under the assumption that the kinetic energy of the system can be approximated by that portion residing within the large payload. These equations were effectively combined with the modified I−O notion to derive a control strategy suitable for this class of manipulators. An adaptive version of the scheme was also developed.[19] These works employed a feedforward based on the payload alone, which subsequent experimental and theoretical work has shown can be improved. For example, the rotor inertias corresponding to highly geared actuators make a contribution to the dynamics which cannot be ignored.

A detailed study[20] of the vibration modes of flexible robots provided us with necessary and sufficient conditions for all modes to exhibit a node at the manipulator's end point: $M_{\theta\theta} J_\theta^{-1} J_e = M_{\theta e}$. It was shown that this property can be closely achieved for large tip−link mass ratio and sufficiently small rotor inertias. The localized nature of the vibration modes can be intuitively understood if we consider the limiting case of an infinitely big payload, which can be effectively interpreted as a clamping boundary condition at the end point. A Lagrangian approach was then employed to derive the dynamic equations

of motion and demonstrate that an effective separation of the task-space dynamics from the elastic ones is possible when massive payloads were involved. The nonlinear torques to end-effector dynamics were shown to become essentially equivalent to the corresponding rigid case,

$$M_{\rho\rho}\ddot{\boldsymbol{\rho}} + C_{\rho}\dot{\boldsymbol{\rho}} = J_{\theta}^{-T}(\boldsymbol{\theta}, \mathbf{q}_e)\boldsymbol{\tau} \quad (6)$$

where

$$M_{\rho\rho} \triangleq J_{\theta}^{-T} M_{\theta\theta} J_{\theta}^{-1}$$
$$C_{\rho}(\boldsymbol{\rho}, \dot{\boldsymbol{\rho}})\dot{\boldsymbol{\rho}} \triangleq \dot{M}_{\rho\rho}\dot{\boldsymbol{\rho}} - \tfrac{1}{2}\partial\left(\dot{\boldsymbol{\rho}}^T M_{\rho\rho}\dot{\boldsymbol{\rho}}\right)/\partial\boldsymbol{\rho} \quad (7)$$

The matrix $M_{\rho\rho}$ is evaluated at the configuration $\boldsymbol{\theta} = \mathbf{F}_r^{-1}(\boldsymbol{\rho})$ and $\mathbf{q}_e = \mathbf{0}$, where $\mathbf{F}_r(\cdot)$ is the rigid forward kinematics map. The matrix C_{ρ} can be constructed so that $(2C_{\rho} - \dot{M}_{\rho\rho})$ is skew-symmetric.

The elastic coordinates were shown to obey

$$\hat{M}_{ee}\ddot{\mathbf{q}}_e + D_{ee}\dot{\mathbf{q}}_e + K_{ee}\mathbf{q}_e = -J_e^T J_{\theta}^{-T}\boldsymbol{\tau} + \mathbf{f}_{\mathrm{non},e} \quad (8)$$

where

$$\hat{M}_{ee} \triangleq M_{ee} - M_{\theta e}^T M_{\theta\theta}^{-1} M_{\theta e} \quad (9)$$

$$\mathbf{f}_{\mathrm{non},e} \triangleq -\left(\dot{\hat{M}}_{ee}\dot{\mathbf{q}}_e - \tfrac{1}{2}\partial\left(\dot{\boldsymbol{\rho}}^T M_{\rho\rho}\dot{\boldsymbol{\rho}}\right)/\partial\mathbf{q}_e \right.$$
$$\left. - \tfrac{1}{2}\partial\left(\dot{\mathbf{q}}_e^T \hat{M}_{ee}\dot{\mathbf{q}}_e\right)/\partial\mathbf{q}_e\right) \quad (10)$$

Suppressing the elastic dependence in $M_{\rho\rho}$ leads to neglecting the second term in $\mathbf{f}_{\mathrm{non},e}$, and the localized nature of the vibration modes advocates forming $\hat{M}_{ee}$ subject to $\dot{\boldsymbol{\rho}} = \mathbf{0}$. The nonlinear terms can then be written as $\mathbf{f}_{\mathrm{non},e} = -C_e(\mathbf{q}, \dot{\mathbf{q}}_e)\dot{\mathbf{q}}_e$, and the matrix C_e can be constructed so that $(2C_e - \dot{\hat{M}}_{ee})$ is skew-symmetric.

It might be useful to repeat a comment made in the original source of the equations[20] and point out an analogy with the results of Sicilano and Book.[21] In that work, a singular perturbation approach was used and a slow and a fast subsystem were identified for the flexible plant. The slow subsystem turned out to be the joint-space dynamics of the corresponding rigid case, whereas here it is the task-space version which plays the equivalent role. The elastic equations in Eq. (8) which are formed subject to $\dot{\boldsymbol{\rho}} = \mathbf{0}$ are analogous to the fast dynamics.

4. PAYLOAD–DOMINATED INVERSE DYNAMICS AND PASSIVE FEEDBACK CONTROLLER

The scheme effectively exploits the above approximate description of the payload-dominated dynamics to extend the ideas presented in previous related work.[18] For the problem of tracking a time-varying trajectory, $\boldsymbol{\rho}_d$, the applied torque can be divided into a feedforward, $\boldsymbol{\tau}_d$, and a feedback part, $\tilde{\boldsymbol{\tau}}$. Equation (6) suggests the following choice for the feedforward:

$$\boldsymbol{\tau} = \boldsymbol{\tau}_d + \tilde{\boldsymbol{\tau}}$$
$$\boldsymbol{\tau}_d = J_{\theta}^T(\boldsymbol{\theta}, \mathbf{q}_e)\left[M_{\rho\rho}(\boldsymbol{\rho})\ddot{\boldsymbol{\rho}}_d + C_{\rho}(\boldsymbol{\rho}, \dot{\boldsymbol{\rho}})\dot{\boldsymbol{\rho}}_d\right] \quad (11)$$

Equation (8) can then be used to define an estimate of the elastic coordinates, $\mathbf{q}_{ed}$, produced by the application of $\boldsymbol{\tau}_d$:

$$\hat{M}_{ee}\ddot{\mathbf{q}}_{ed} + D_{ee}\dot{\mathbf{q}}_{ed} + K_{ee}\mathbf{q}_{ed} + C_e(\mathbf{q}, \dot{\mathbf{q}}_e)\dot{\mathbf{q}}_{ed}$$
$$= -J_e^T J_{\theta}^{-T}\boldsymbol{\tau}_d \quad (12)$$

Given $\mathbf{q}_{ed}$ and the expression for $\dot{\boldsymbol{\rho}}_{\mu}$ in Eq. (5), the desired trajectory $\dot{\boldsymbol{\rho}}_{\mu d}$ is defined as

$$\dot{\boldsymbol{\rho}}_{\mu d} = \dot{\boldsymbol{\rho}}_d - (1 - \mu)J_e(\boldsymbol{\theta}, \mathbf{q}_e)\dot{\mathbf{q}}_{ed} \quad (13)$$

and the error trajectory for $\dot{\boldsymbol{\rho}}_{\mu}$ becomes

$$\dot{\tilde{\boldsymbol{\rho}}}_{\mu} = \dot{\boldsymbol{\rho}}_{\mu} - \dot{\boldsymbol{\rho}}_{\mu d} = \dot{\tilde{\boldsymbol{\rho}}} - (1 - \mu)J_e\dot{\tilde{\mathbf{q}}}_e \quad (14)$$

where $\tilde{\boldsymbol{\rho}} \triangleq \boldsymbol{\rho} - \boldsymbol{\rho}_d$ and $\tilde{\mathbf{q}}_e \triangleq \mathbf{q}_e - \mathbf{q}_{ed}$. It is important to emphasize[18] that $\dot{\tilde{\boldsymbol{\rho}}}_{\mu} \equiv \mathbf{0}$ and $\tilde{\mathbf{q}}_e \equiv \mathbf{0}$ result in $\tilde{\boldsymbol{\rho}} \equiv \mathbf{0}$.

Substituting Eq. (11) into (6) and subtracting (12) from (8), the following description of the tracking error dynamics is obtained

$$M_{\rho\rho}(\boldsymbol{\rho})\ddot{\tilde{\boldsymbol{\rho}}} + C_{\rho}(\boldsymbol{\rho}, \dot{\boldsymbol{\rho}})\dot{\tilde{\boldsymbol{\rho}}} = J_{\theta}^{-T}\tilde{\boldsymbol{\tau}} \quad (15)$$

$$\hat{M}_{ee}\ddot{\tilde{\mathbf{q}}}_e + D_{ee}\dot{\tilde{\mathbf{q}}}_e + K_{ee}\tilde{\mathbf{q}}_e + C_e(\mathbf{q}, \dot{\mathbf{q}}_e)\dot{\tilde{\mathbf{q}}}_e = -J_e^T J_{\theta}^{-T}\tilde{\boldsymbol{\tau}} \quad (16)$$

Theorem 1: *The mapping* $\dot{\tilde{\boldsymbol{\rho}}}_{\mu} = G(J_{\theta}^{-T}\tilde{\boldsymbol{\tau}})$ *is passive for* $\mu < 1$.

Proof: Define the nonnegative function S_{μ}:

$$S_{\mu} = \tfrac{1}{2}\dot{\tilde{\boldsymbol{\rho}}}^T M_{\rho\rho}\dot{\tilde{\boldsymbol{\rho}}} + \tfrac{1}{2}(1 - \mu)\left[\dot{\tilde{\mathbf{q}}}_e^T \hat{M}_{ee}\dot{\tilde{\mathbf{q}}}_e + \tilde{\mathbf{q}}_e^T K_{ee}\tilde{\mathbf{q}}_e\right]$$
$$\mu < 1 \quad (17)$$

Differentiating with respect to time and using Eqs. (15), (16), and the skew-symmetry property of the matrices $(2C_\rho - \dot{M}_{\rho\rho})$ and $(2C_e - \dot{M}_{ee})$ gives

$$
\begin{aligned}
\dot{S}_\mu &= \dot{\hat{\rho}}^T \left[M_{\rho\rho}\ddot{\hat{\rho}} + \tfrac{1}{2}\dot{M}_{\rho\rho}\dot{\hat{\rho}} \right] + (1-\mu) \\
&\quad \times \dot{\hat{q}}_e^T \left[\hat{M}_{ee}\ddot{\hat{q}}_e + \tfrac{1}{2}\dot{\hat{M}}_{ee}\dot{\hat{q}}_e + K_{ee}\tilde{q}_e \right] \\
&= \left[\dot{\hat{\rho}} + (1-\mu)J_e\dot{\hat{q}}_e \right]^T J_\theta^{-T}\tilde{\tau} - (1-\mu)\dot{\hat{q}}_e^T D_{ee}\dot{\hat{q}}_e \\
&= \dot{\hat{\rho}}_\mu^T \left(J_\theta^{-T}\tilde{\tau} \right) - (1-\mu)\dot{\hat{q}}_e^T D_{ee}\dot{\hat{q}}_e
\end{aligned}
\tag{18}
$$

Integrating the above and setting $S_\mu(0) = 0$ establishes the result for $\mu < 1$:

$$
\int_0^T \dot{\hat{\rho}}_\mu^T \left(J_\theta^{-T}\tilde{\tau} \right) dt = S_\mu(T) - S_\mu(0) + (1-\mu)\dot{\hat{q}}_e^T D_{ee}\dot{\hat{q}}_e
$$

$$
\geq S_\mu(T) \tag{19}
$$

∎

4.1. Feedback Design

Since the modified I–O plant preserves the passivity property in the error dynamics using the indicated feedforward, the passivity theorem guarantees that any strictly passive feedback compensator stabilizes the system. The very simple proportional-derivative (PD) controller provides a suitable choice,

$$
\tilde{\tau} = -J_\theta^T(\theta, q_e)\left[K_p\tilde{\rho}_\mu + K_d\dot{\tilde{\rho}}_\mu \right] \tag{20}
$$

where K_p, K_d are symmetric positive-definite matrices.

Global asymptotic stability of the closed-loop system can be proved by employing the following Lyapunov function:

$$
V = S_\mu + \tfrac{1}{2}\tilde{\rho}_\mu^T K_p\tilde{\rho}_\mu \geq 0 \qquad \mu < 1 \tag{21}
$$

Using the previous theorem, $\dot{V} = -\dot{\tilde{\rho}}_\mu^T K_d\dot{\tilde{\rho}}_\mu - (1-\mu)\dot{\hat{q}}_e^T D_{ee}\dot{\hat{q}}_e \leq 0$ and applying the same arguments as used in the predecessor of the scheme[18] yields the result. The combined feedforward–feedback controller becomes

$$
\tau(t) = J_\theta^T(\theta, q_e)\left[M_{\rho\rho}(\rho)\ddot{\rho}_d + C_\rho(\rho, \dot{\rho})\dot{\rho}_d \right]
$$

$$
- J_\theta^T(\theta, q_e)\left[K_d\dot{\tilde{\rho}}_\mu + K_p\tilde{\rho}_\mu \right] \tag{22}
$$

4.2. Joint-Based Implementation of the Feedforward

Implementing the feedforward part of the scheme requires the calculation of the task-space dynamic equations, which can be a nontrivial task in the multilink case. As an alternative, we propose the use of a set of "fictitious" joint quantities to be used in conjunction with the corresponding joint-based dynamic equations which are easier to construct.

It is known that for a rigid robot the task-space dynamic equations are related to the equivalent joint-space ones as[22]

$$
M_{\rho\rho}(\rho) = J_\theta^{-T}(\theta_t, 0)M_{\theta\theta}(\theta_t)J_\theta^{-1}(\theta_t, 0) \tag{23}
$$

$$
C_\rho(\rho, \dot{\rho}) = J_\theta^{-T}\left[C_\theta(\theta_t, \dot{\theta}_t) - M_{\theta\theta}J_\theta^{-1}\dot{J}_\theta \right]J_\theta^{-1} \tag{24}
$$

where $M_{\theta\theta}$ (only joint angle dependence here) and C_θ are the corresponding joint-space mass and nonlinear terms matrices, respectively. All matrix quantities on the right-hand side (RHS) of the above equations are evaluated at the rigid inverse kinematics configuration $\theta_t = F_r^{-1}(\rho)$, $\dot{\theta}_t = J_\theta^{-1}(\theta_t, 0)\dot{\rho}$.

We assume that singular configurations are avoided and define the fictitious desired joint trajectories, $\theta_d(t)$, using the relation $\dot{\rho}_d = J_\theta(\theta_t, 0)\dot{\theta}_d$ so that

$$
\dot{\theta}_d \triangleq J_\theta^{-1}(\theta_t, 0)\dot{\rho}_d \tag{25}
$$

$$
\ddot{\theta}_d \triangleq J_\theta^{-1}(\theta_t, 0)\left[\ddot{\rho}_d - \dot{J}_\theta(\theta_t, 0)\dot{\theta}_d \right] \tag{26}
$$

The feedforward part of the controller becomes

$$
\tau_d = J_\theta^T(\theta, q_e)J_\theta^{-T}(\theta_t, 0)\left[M_{\theta\theta}(\theta_t)\ddot{\theta}_d + C_\theta(\theta_t, \dot{\theta}_t)\dot{\theta}_d \right] \tag{27}
$$

which is equivalent to that in Eq. (11). The joint-space implementation will be especially useful in the adaptive context.

5. ADAPTIVE CONTROLLER

One very common problem in robotic control is uncertainty involving the mass properties of the arm or the grasped object. Adaptive techniques provide an attractive option for consistent performance in the presence of unknown or poorly defined parameters. Many globally stable adaptive control techniques have been proposed for the rigid robot case. Ortega and Spong[15] provide a collection of

some of the most significant ones in a unified tutorial form. Important properties for the development of such schemes are the linear dependence of a model-based feedforward law on a set of suitably defined parameters, and the passivity of the torque to joint-rates map.

In the context of flexible-link robots, Damaren[19] created a framework suitable for adaptive controller design by effectively exploiting the payload-dominated equations of motion in conjunction with their passivity property. The scheme permitted only the properties of the payload to be estimated on-line. An important extension is presented here, constructed upon Eqs. (6) and (8), which includes the mass properties of the robot itself in the set of adaptively updated parameters. The controller architecture consists of a control law coupled with a parameter update law which extracts parameter information from the tracking errors so that performance improves with time.

5.1. Fixed Parameter Control Law

As a first step in developing the adaptive scheme, Eq. (6) suggests the following feedforward law for the known parameter case,

$$\boldsymbol{\tau}_d = J_\theta^T W(\ddot{\boldsymbol{\rho}}_d, \dot{\boldsymbol{\rho}}_d, \dot{\boldsymbol{\rho}}, \boldsymbol{\rho})\boldsymbol{\alpha}$$
$$W(\ddot{\boldsymbol{\rho}}_d, \dot{\boldsymbol{\rho}}_d, \dot{\boldsymbol{\rho}}, \boldsymbol{\rho})\boldsymbol{\alpha} = M_{\rho\rho}(\boldsymbol{\rho})\ddot{\boldsymbol{\rho}}_d + C_\rho(\boldsymbol{\rho}, \dot{\boldsymbol{\rho}})\dot{\boldsymbol{\rho}}_d \quad (28)$$

which can be expressed as a linear function of suitably defined parameters. W is called the regressor matrix and $\boldsymbol{\alpha}$ is the vector of parameters to be adaptively updated.

An estimate for the elastic displacements was given earlier in (12), and the reference trajectory for $\boldsymbol{\rho}_\mu, \boldsymbol{\rho}_{\mu d}$, together with the corresponding tracking errors $\tilde{\boldsymbol{\rho}}_\mu$ and $\dot{\tilde{\boldsymbol{\rho}}}_\mu$ were defined by Eqs. (13) and (14), respectively. The filtered position rates, $\dot{\boldsymbol{\rho}}_r$, and the filtered errors, s_μ, (which can be thought of as a measure of tracking accuracy) are defined as

$$\dot{\boldsymbol{\rho}}_r \triangleq \dot{\boldsymbol{\rho}}_d - \boldsymbol{\Lambda}\tilde{\boldsymbol{\rho}}_\mu \qquad s_\mu \triangleq \dot{\tilde{\boldsymbol{\rho}}}_\mu + \boldsymbol{\Lambda}\tilde{\boldsymbol{\rho}}_\mu \quad (29)$$

with $\boldsymbol{\Lambda} = \boldsymbol{\Lambda}^T > \mathbf{O}$ being a weighting matrix. The filtered output idea was borrowed from the adaptive scheme of Slotine and Li[23,24] for rigid robots. It was introduced to guarantee the convergence of the tracking errors to zero. It is important to emphasize[19] that $s_\mu \in L_2$ implies that $\tilde{\boldsymbol{\rho}}_\mu(t) \in L_2 \cap L_\infty$, $\dot{\tilde{\boldsymbol{\rho}}}_\mu(t) \in L_2$, and $\tilde{\boldsymbol{\rho}}_\mu(t) \to \mathbf{0}$ as $t \to \infty$. Furthermore, if $s_\mu(t) \to \mathbf{0}$ as $t \to \infty$, then $\dot{\tilde{\boldsymbol{\rho}}}_\mu(t) \to \mathbf{0}$.

The errors for the filtered rates and filtered positions are defined by

$$\tilde{\boldsymbol{\rho}}_r \triangleq \boldsymbol{\rho} - \boldsymbol{\rho}_r$$
$$\dot{\tilde{\boldsymbol{\rho}}}_r \triangleq \dot{\boldsymbol{\rho}} - \dot{\boldsymbol{\rho}}_r = \dot{\tilde{\boldsymbol{\rho}}} + \boldsymbol{\Lambda}\tilde{\boldsymbol{\rho}}_\mu \quad (30)$$

Replacing $\boldsymbol{\rho}_d$ with $\boldsymbol{\rho}_r$ in the fixed parameter feedforward gives

$$\boldsymbol{\tau}_d = J_\theta^T W(\ddot{\boldsymbol{\rho}}_r, \dot{\boldsymbol{\rho}}_r, \dot{\boldsymbol{\rho}}, \boldsymbol{\rho})\boldsymbol{\alpha}$$
$$= J_\theta^T \left[M_{\rho\rho}(\boldsymbol{\rho})\ddot{\boldsymbol{\rho}}_r + C_\rho(\boldsymbol{\rho}, \dot{\boldsymbol{\rho}})\dot{\boldsymbol{\rho}}_r \right] \quad (31)$$

and a description of the tracking error dynamics is obtained by subtracting Eq. (31) from (6), and (12) from (8),

$$M_{\rho\rho}(\boldsymbol{\rho})\ddot{\tilde{\boldsymbol{\rho}}}_r + C_\rho(\boldsymbol{\rho}, \dot{\boldsymbol{\rho}})\dot{\tilde{\boldsymbol{\rho}}}_r = J_\theta^{-T}\tilde{\boldsymbol{\tau}} \qquad \tilde{\boldsymbol{\tau}} \triangleq \boldsymbol{\tau} - \boldsymbol{\tau}_d \quad (32)$$

$$\hat{M}_{ee}\ddot{\tilde{\mathbf{q}}}_e + D_{ee}\dot{\tilde{\mathbf{q}}}_e + K_{ee}\tilde{\mathbf{q}}_e = -J_e^T J_\theta^{-T}\tilde{\boldsymbol{\tau}} - C_e(\mathbf{q}, \dot{\mathbf{q}}_e)\dot{\tilde{\mathbf{q}}}_e$$
$$\tilde{\mathbf{q}}_e \triangleq \mathbf{q}_e - \mathbf{q}_{ed} \quad (33)$$

Here, it will be convenient to consider the system as being a mapping from $J_\theta^{-T}\tilde{\boldsymbol{\tau}}$ to s_μ. Ortega et al.,[16] indicate that the use of filtered error effectively reduces the relative degree of the output of the system to one and opens the door to a passivity-based adaptive control approach.

Theorem 2: *The mapping $s_\mu = G(J_\theta^{-T}\tilde{\boldsymbol{\tau}})$ is passive for $\mu < 1$.*

Proof: Define the nonnegative function

$$S_\mu = \tfrac{1}{2}\dot{\tilde{\boldsymbol{\rho}}}_r^T M_{\rho\rho}\dot{\tilde{\boldsymbol{\rho}}}_r + \tfrac{1}{2}(1-\mu)\left[\dot{\tilde{\mathbf{q}}}_e^T \hat{M}_{ee}\dot{\tilde{\mathbf{q}}}_e + \tilde{\mathbf{q}}_e^T K_{ee}\tilde{\mathbf{q}}_e\right]$$
$$\mu < 1 \quad (34)$$

Differentiating with respect to time and using Eqs. (32), (33), and the skew-symmetry property of the matrices $(2C_\rho - \dot{M}_{\rho\rho})$ and $(2C_e - \dot{\hat{M}}_{ee})$ gives

$$\dot{S}_\mu = \dot{\tilde{\boldsymbol{\rho}}}_r^T\left[M_{\rho\rho}\ddot{\tilde{\boldsymbol{\rho}}}_r + \tfrac{1}{2}\dot{M}_{\rho\rho}\dot{\tilde{\boldsymbol{\rho}}}_r\right] + (1-\mu)$$
$$\times \dot{\tilde{\mathbf{q}}}_e^T\left[\hat{M}_{ee}\ddot{\tilde{\mathbf{q}}}_e + \tfrac{1}{2}\dot{\hat{M}}_{ee}\dot{\tilde{\mathbf{q}}}_e + K_{ee}\tilde{\mathbf{q}}_e\right]$$
$$= \left[\dot{\tilde{\boldsymbol{\rho}}}_r - (1-\mu)J_e\dot{\tilde{\mathbf{q}}}_e\right]^T J_\theta^{-T}\tilde{\boldsymbol{\tau}} - (1-\mu)\dot{\tilde{\mathbf{q}}}_e^T D_{ee}\dot{\tilde{\mathbf{q}}}_e$$
$$= s_\mu^T\left(J_\theta^{-T}\tilde{\boldsymbol{\tau}}\right) - (1-\mu)\dot{\tilde{\mathbf{q}}}_e^T D_{ee}\dot{\tilde{\mathbf{q}}}_e \quad (35)$$

Integrating the above gives $\int_0^T s_\mu^T(J_\theta^{-T}\tilde{\boldsymbol{\tau}})\,dt \geq S_\mu(T) - S_\mu(0)$ and setting $S_\mu(0) = 0$ establishes the result upon noting that $S_\mu \geq 0$ when $\mu < 1$. ∎

5.2. Adaptive Version

The feedback part of the controller is selected so that the passivity theorem is satisfied

$$\tilde{\boldsymbol{\tau}} = -J_\theta^T(\boldsymbol{\theta}, \mathbf{q}_e)Hs_\mu$$

$$\int_0^T s_\mu^T Hs_\mu\,dt \geq \epsilon \int_0^T s_\mu^T s_\mu\,dt \qquad (36)$$

$$\forall T > 0$$

for some constant $\epsilon > 0$, i.e., H is a strictly passive operator. A controller suitable for trajectory following often consists of a feedforward and a feedback part, $\bar{\boldsymbol{\tau}}(t)$. Since the parameters $\boldsymbol{\alpha}$ are unknown, the applied torque is taken to be

$$\boldsymbol{\tau} = J_\theta^T W(\ddot{\boldsymbol{\rho}}_r, \dot{\boldsymbol{\rho}}_r, \dot{\boldsymbol{\rho}}, \boldsymbol{\rho})\hat{\boldsymbol{\alpha}} + \bar{\boldsymbol{\tau}}(t) \qquad (37)$$

with $\hat{\boldsymbol{\alpha}}(t)$ the vector of parameter estimates.

Subtracting Eq. (31) from (37) yields

$$\tilde{\boldsymbol{\tau}} = \boldsymbol{\tau} - \boldsymbol{\tau}_d = J_\theta^T W\tilde{\boldsymbol{\alpha}} + \bar{\boldsymbol{\tau}}$$

$$\tilde{\boldsymbol{\alpha}}(t) \triangleq \hat{\boldsymbol{\alpha}}(t) - \boldsymbol{\alpha} \qquad (38)$$

and hence,

$$\int_0^T \left(J_\theta^{-T}\tilde{\boldsymbol{\tau}}\right)^T s_\mu\,dt = \int_0^T \tilde{\boldsymbol{\alpha}}^T W^T s_\mu\,dt + \int_0^T \left(J_\theta^{-T}\bar{\boldsymbol{\tau}}\right)^T s_\mu\,dt \qquad (39)$$

If $\tilde{\boldsymbol{\alpha}}$ is chosen to be a passive function of $-W^T s_\mu(t)$ and the map from $-s_\mu$ to $J_\theta^{-T}\bar{\boldsymbol{\tau}}$ is strictly passive, then H in Eq. (36) will be a strictly passive operator. These observations suggest the following control and parameter update laws,

$$\boldsymbol{\tau}(t) = J_\theta^T(\boldsymbol{\theta}, \mathbf{q}_e)W(\ddot{\boldsymbol{\rho}}_r, \dot{\boldsymbol{\rho}}_r, \dot{\boldsymbol{\rho}}, \boldsymbol{\rho})\hat{\boldsymbol{\alpha}}(t) - J_\theta^T(\boldsymbol{\theta}, \mathbf{q}_e)K_d s_\mu$$

$$K_d = K_d^T > \mathbf{O} \qquad (40)$$

$$\dot{\hat{\boldsymbol{\alpha}}} = \dot{\tilde{\boldsymbol{\alpha}}} = -\boldsymbol{\Gamma}W^T s_\mu \qquad \boldsymbol{\Gamma} = \boldsymbol{\Gamma}^T > \mathbf{O} \qquad (41)$$

Our adaptive algorithm yields global asymptotic stability for the tracking errors $\tilde{\boldsymbol{\rho}}$ and $\dot{\tilde{\boldsymbol{\rho}}}$ for $\mu < 1$. To prove the above statement, the following Lyapunov function can be used in conjunction with the same arguments expressed in the earliest ver-

sion[19] of the scheme,

$$V(t) = S_\mu + \tfrac{1}{2}\tilde{\boldsymbol{\alpha}}^T \boldsymbol{\Gamma}^{-1}\tilde{\boldsymbol{\alpha}} \geq 0 \qquad (42)$$

$$\dot{V}(t) = s_\mu^T\left[J_\theta^{-T}\tilde{\boldsymbol{\tau}} - W\tilde{\boldsymbol{\alpha}}\right] - (1 - \mu)\dot{\tilde{\mathbf{q}}}_e^T D_{ee}\dot{\tilde{\mathbf{q}}}_e$$

$$= -s_\mu^T K_d s_\mu - (1 - \mu)\dot{\tilde{\mathbf{q}}}_e^T D_{ee}\dot{\tilde{\mathbf{q}}}_e \leq 0 \qquad (43)$$

Based on the previous work, it is clear that the stability and the convergence of the tracking errors to zero is independent of the convergence of the parameter estimates to their exact values. As is very common for many adaptive schemes, such convergence requires that the trajectories are persistently exciting (PE). Of course such parametric convergence hinges on the requirement that the regressor matrix is constructed using an exact model for the plant. The PE property, although not a necessary condition, is in general desirable. For the case of non-PE trajectories, the parameters evolve in such a way that the control objectives are achieved.

Our scheme is an example of adaptive algorithms which effectively exploit the known structure of the system dynamics. By constructing the regressor matrix, we effectively focus upon a family of candidate models that describe the plant. Then, the adaptation is responsible for selecting the particular member of the family which best represents the plant. Another interesting remark to be made is that for a value of $\mu = 0$, the scheme reduces to the task-space version of the adaptive algorithm for rigid robots of Slotine and Li.[23]

5.3. Joint-Based Parametrization of the Regressor

Constructing the regressor matrix using parametrization in task-space coordinates can be a very difficult exercise, and this problem can be overcome in a similar fashion to the nonadaptive case by using a suitable transformation. The fictitious joint quantities, $\boldsymbol{\theta}_r(t)$, are defined by $\dot{\boldsymbol{\rho}}_r = J_\theta(\boldsymbol{\theta}_t, 0)\dot{\boldsymbol{\theta}}_r$ so that

$$\dot{\boldsymbol{\theta}}_r \triangleq J_\theta^{-1}(\boldsymbol{\theta}_t, 0)\dot{\boldsymbol{\rho}}_r \qquad (44)$$

$$\ddot{\boldsymbol{\theta}}_r = J_\theta^{-1}(\boldsymbol{\theta}_t, 0)\left[\ddot{\boldsymbol{\rho}}_r - \dot{J}_\theta(\boldsymbol{\theta}_t, 0)\dot{\boldsymbol{\theta}}_r\right] \qquad (45)$$

Given the above definitions,

$$M_{\rho\rho}(\boldsymbol{\rho})\ddot{\boldsymbol{\rho}}_r + C_\rho(\boldsymbol{\rho}, \dot{\boldsymbol{\rho}})\dot{\boldsymbol{\rho}}_r$$

$$= J_\theta^{-T}(\boldsymbol{\theta}_t, 0)\left[M_{\theta\theta}(\boldsymbol{\theta}_t)\ddot{\boldsymbol{\theta}}_r + C_\theta(\boldsymbol{\theta}_t, \dot{\boldsymbol{\theta}}_t)\dot{\boldsymbol{\theta}}_r\right] \qquad (46)$$

or

$$W(\ddot{\boldsymbol{\rho}}_r, \dot{\boldsymbol{\rho}}_r, \dot{\boldsymbol{\rho}}, \boldsymbol{\rho})\boldsymbol{\alpha} = J_\theta^{-T}(\boldsymbol{\theta}_t, 0)Y(\ddot{\boldsymbol{\theta}}_r, \dot{\boldsymbol{\theta}}_r, \dot{\boldsymbol{\theta}}_t, \boldsymbol{\theta}_t)\boldsymbol{\alpha} \quad (47)$$

with Y the corresponding joint-based rigid version of the regressor matrix. Then, the applied torque and the adaptation law become

$$\boldsymbol{\tau}(t) = J_\theta^T(\boldsymbol{\theta}, \mathbf{q}_e) J_\theta^{-T}(\boldsymbol{\theta}_t, 0)Y(\ddot{\boldsymbol{\theta}}_r, \dot{\boldsymbol{\theta}}_r, \dot{\boldsymbol{\theta}}_t, \boldsymbol{\theta}_t)\hat{\boldsymbol{\alpha}}(t)$$
$$- J_\theta^T(\boldsymbol{\theta}, \mathbf{q}_e)K_d s_\mu \quad (48)$$

$$\dot{\hat{\boldsymbol{\alpha}}} = -\boldsymbol{\Gamma} Y^T J_\theta^{-1}(\boldsymbol{\theta}_t, 0)s_\mu \quad (49)$$

The transformation introduced here allows parametrizing the regressor matrix in joint coordinates, which is much easier to construct since the Jacobian matrix relating the joint coordinates to the task-space one is effectively eliminated from the formulation. In the case of a rigid robot, it reduces to the transformation suggested for the Cartesian-space implementation of Slotine and Li's[23] algorithm. In a rigid context, it is similar to the one Fossen[25] proposed for the adaptive control of a spacecraft, to achieve a parametrization of the regressor in terms of the body frame rather than the inertial frame coordinates.

6. ASSUMPTIONS AND IMPLEMENTATION ISSUES

When implementing the above class of controllers, direct measurements of the elastic coordinates $\mathbf{q}_e$ are required for the construction of the μ-tip position and rate and the Jacobian matrix $J_\theta(\boldsymbol{\theta}, \mathbf{q}_e)$ as well. To avoid these problems, the following simplifications[18] will be incorporated in our implementation examples,

$$J_\theta(\boldsymbol{\theta}, \mathbf{q}_e) \doteq J_\theta(\boldsymbol{\theta}, 0)$$
$$\dot{\boldsymbol{\rho}}_{\mu d} \doteq \dot{\boldsymbol{\rho}}_d \qquad \boldsymbol{\rho}_{\mu d} \doteq \boldsymbol{\rho}_d \quad (50)$$

so that $\dot{\tilde{\boldsymbol{\rho}}}_\mu(t) \doteq [\mu\dot{\boldsymbol{\rho}}(t) + (1-\mu)J_\theta(\boldsymbol{\theta}, 0)\dot{\boldsymbol{\theta}}(t)] - \dot{\boldsymbol{\rho}}_d(t)$ and $\tilde{\boldsymbol{\rho}}_\mu(t) \doteq [\mu\boldsymbol{\rho}(t) + (1-\mu)\mathbf{F}_r(\boldsymbol{\theta})] - \boldsymbol{\rho}_d(t)$. Using the above, we have also removed the need to calculate the trajectories for the elastic coordinates $\mathbf{q}_{ed}$ and $\dot{\mathbf{q}}_{ed}$ as defined earlier in Eq. (12). On the basis of our numerical simulations and experimental experience, an appropriate value for μ is very close to 1, which supports the validity of the above simplifications.

7. EXPERIMENTAL RESULTS

7.1. The Experimental Facility

Experimental results involving flexible-link robots are of great value since flimsy-link space robots can undergo limited testing prior to launch. Unlike most of the experimental work carried out in the field, which has focused on the one-link setup or with two links of which only one is flexible, our experiments involve the more realistic three-link configuration with two flexible links. This is an important excursion from single-link results since the multibody nonlinearities are significant.

Our facility, which is shown in Figure 1, was designed and built in the Department of Mechanical Engineering at the University of Canterbury and consists of two robotic arms possessing three rotational DOF and two flexible links each. The arms are constrained to move in the horizontal plane so that gravity effects are not considered. The modular design of the facility allows a variety of experiments to be performed using different geometries and combinations of rigid and/or flexible links. Each arm is supported on air-pads floating on a glass-topped table in an almost frictionless fashion.

A specially designed payload can be rigidly attached to the tip of each arm, and both its mass and moment of inertia can be varied. Multiple connections on the payload allow both arms to be connected to it simultaneously, and experiments performed with closed-loop configurations as well. Geared actuation is used and each motor is equipped with incremental encoders which provide accurate rotation measurements. No direct velocity information is available and when needed is obtained by simple differencing of the position signals. Consequently, the available velocity signals were contaminated with noise, and filtering using low-order Butterworth techniques was employed to considerably improve their quality.

Tip measurements are also required for the implementation of our schemes. Although such information can be provided by any suitable vision system, a method based on strain-gauges is preferable due to its simplicity, low cost, and compactness. This method was successfully utilized for implementing our controllers. A set of k strain-gauges were attached on each flexible link at discrete positions along its length and static loading was used for calibrating them to provide strain measurements. An nth order polynomial was assumed to describe the deflected shape of each flexible link
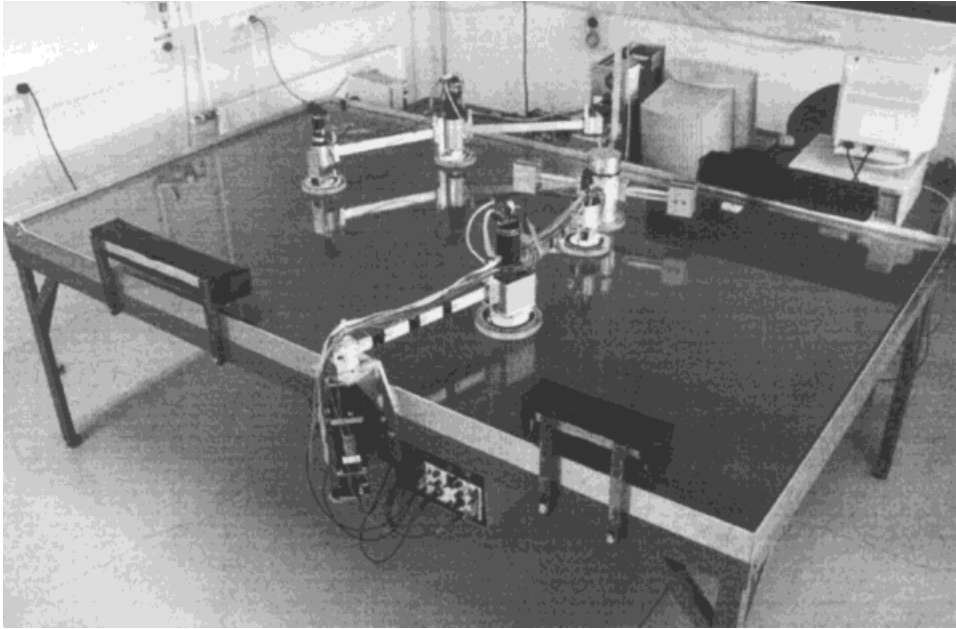
Figure 1. The experimental facility.

and therefore capture an equal number of vibration modes. Given the success of cantilevered shape functions when used in conjunction with the assumed modes method in modeling our system, polynomials satisfying clamped boundary conditions at the base were selected,

$$U_e(x, t) = q_{e,1} x^2 + q_{e,2} x^3 + \cdots + q_{e,n-1} x^n$$
$$n \le k + 1 \quad (51)$$

with U_e the deflection and x the distance along the undeflected axis of the link.

Mechanics of materials theory provides the strain-curvature relation for a flexible beam: $\varepsilon(x, t) = -(b/2) \partial^2 U_e(x, t) / \partial x^2$, where b is its thickness. Evaluating ε at each of the k measurement sites gives a linear system of simultaneous equations, the solution of which provides a set of elastic DOF for the arm. When $n < k + 1$ the problem is overdetermined and a pseudoinverse least-squares solution for the system can be used. Forward kinematics can then be applied to give the position of the end point, and tip velocity measurements become available by differencing the position signals. It is noted that such a method is suited to implementing controllers requiring full state feedback.

In the present case, three sets of strain-gauges were evenly distributed along the length of each flexible link, ($k = 3$), and third-order polynomials were considered, ($n = 3$). The accuracy of the method was assessed using a two-dimensional charge coupled device (CCD) camera located above the table. The measurements obtained were also found to be in good agreement with the simulated behavior of the controlled motion. Experimental results involving such a method were reported by Hastings and Book,[26] and investigations of a similar approach were made by Miller and Piedboeuf.[27]

For the arm under examination, the two flexible links are aluminum beams of cross-section 6×30 mm. Due to the design geometry of the arm, mechanical offsets exist between the connection of flexible links and actuators. These offsets correspond to extra rigid links that have to be modeled as part of the chain. Consequently, our arm consists of seven interconnected bodies, two of which are flexible, and a large payload attached to the end of the chain. Their mass properties were calculated using solid models produced with computer-aided design (CAD) software. They are collected in Table I, where l is the length, m is the mass, c_x is the first moment of inertia measured along its length, and I is the second moment of inertia about the vertical axis. All properties refer to a frame rigidly attached to the inboard end of the body. The rotor inertias as "seen" at the output shaft of each gearbox are 127.8, 306.9, and 16.1 g m^{-2}, respectively.

Table I. Mass properties of the arm.

Body	l (mm)	m (kg)	I (g m^2)	c_x (g m^{-1})
1	37	2.53	0.12	1.61
2	392	0.19	9.79	37.48
3	77	2.23	14.93	161.77
4	112	2.10	4.60	29.52
5	327	0.16	5.69	26.08
6	66.7	0.93	4.15	54.61
7	70	0.97	1.67	9.36
Payload	—	8.66	480.36	971.03

The control of the system is based on a personal computer (PC) and a high-speed digital signal processor (DSP) connected to the PC bus, allowing for the execution of complex control algorithms at fast sampling rates as required by real-time applications. For our experiments, the sampling frequency was selected to be 200 Hz.

7.2. Desired Trajectories

For our nonadaptive example, the desired end-effector trajectory, $\boldsymbol{\rho}_d$, was taken to be such that all three end-effector DOF follow a quintic polynomial between an initial position, $\boldsymbol{\rho}_i$, and a final position, $\boldsymbol{\rho}_f$, in a certain length of time, t_f. Such trajectories are smooth both in velocities and accelerations and are commonly used in rigid robot trajectory planning:

$$\boldsymbol{\rho}_d(t) = \left[10\left(\frac{t}{t_f}\right)^3 - 15\left(\frac{t}{t_f}\right)^4 + 6\left(\frac{t}{t_f}\right)^5\right](\boldsymbol{\rho}_f - \boldsymbol{\rho}_i) + \boldsymbol{\rho}_i$$

(52)

The initial position is taken to be the one that corresponds to the rigid joint configuration

$$\boldsymbol{\theta}_i = \left[-\frac{\pi}{8} \quad \frac{\pi}{4} \quad 0\right]^T \text{ rad}$$

and the final one to

$$\boldsymbol{\theta}_f = \left[\frac{\pi}{8} \quad \frac{7\pi}{16} \quad \frac{\pi}{3}\right]^T \text{ rad}$$

The duration of the motion is taken to be $t_f = 3$ s.

For our adaptive example, the desired task-space trajectory is the one the corresponding rigid robot would follow if all the joints were tracing a fifth-order polynomial between an initial joint configuration, $\boldsymbol{\theta}_i$, and a final joint configuration, $\boldsymbol{\theta}_f$, in a

certain length of time, t_f,

$$\boldsymbol{\rho}_d(t) = \mathbf{F}_r(\bar{\boldsymbol{\theta}}_d)$$

(53)

$$\bar{\boldsymbol{\theta}}_d(t) = \left[10\left(\frac{t}{t_f}\right)^3 - 15\left(\frac{t}{t_f}\right)^4 + 6\left(\frac{t}{t_f}\right)^5\right](\boldsymbol{\theta}_f - \boldsymbol{\theta}_i) + \boldsymbol{\theta}_i$$

(54)

with

$$\boldsymbol{\theta}_i = \left[\frac{\pi}{4} \quad \frac{\pi}{4} \quad 0\right]^T \text{ rad}$$

$$\boldsymbol{\theta}_f = \left[\frac{7\pi}{16} \quad \frac{7\pi}{16} \quad \frac{\pi}{3}\right]^T \text{ rad}$$

and $t_f = 3$ s. The maneuver was used in a periodic fashion to allow enough time for learning and better demonstrate the merits of adaptation. Between each reversal a 3 s resting time was considered.

7.3. Rigid Inverse Dynamics Feedforward and Passive Feedback Scheme

A suitable choice for the feedback gains is a diagonal matrix with positive entries. For this example, we used $\boldsymbol{K}_p = \text{diag}\{420 \text{ N/m}, 560 \text{ N/m}, 16.8 \text{ N} - \text{m/rad}\}$ and $\boldsymbol{K}_d = \text{diag}\{12 \text{ N/m s}^{-1}, 16 \text{ N/m s}^{-1}, 0.48 \text{ N} - \text{m/rad s}^{-1}\}$. In Figure 2, the three graphs at the top show the tip position tracking corresponding to each one of the three controlled task-space DOF, for a value of $\mu = 0.92$. The continuous line represents the actual task-space trajectory and the dashed line is the desired one. Very good tracking is evident, without any residual vibrations after the completion of the useful motion. The corresponding tracking errors are shown in Figure 3.

The three graphs at the bottom of Figure 2 show the corresponding joint-space tracking with the solid line being the actual joint motion, and the dashed one is the trajectory that the corresponding rigid robot would have to follow to yield the same desired task-space one. It is not surprising that the two trajectories are different, as the end-point position depends not only on the joint rotations, but on the link deflections as well. This fact clearly explains why the schemes traditionally used in controlling rigid robots are not suitable for the flexible-link case.

In Figure 4, one can see the velocity tracking for both the task and the joint-space degrees of freedom, which provide us with additional information about the tracking and vibration damping capabilities of the controller. Furthermore, the velocity
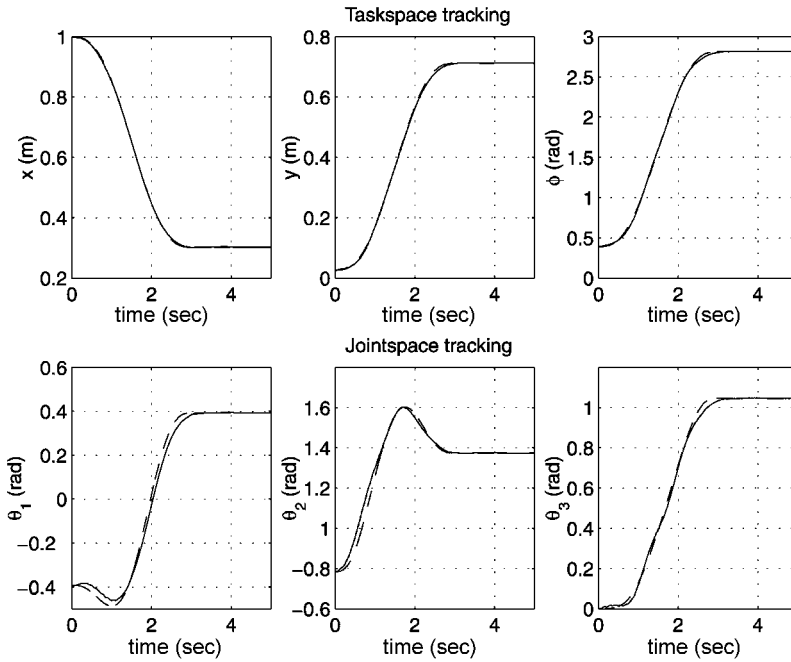
Figure 2. Tracking for the rigid inverse dynamics and passive feedback scheme (dashed line, desired−rigid, solid line, actual).

graphs convey important information about the stability of the system, since any instabilities manifest themselves first at the rates. Once again, we see that the desired task-space trajectories were well traced and that such action translates to joint trajectories different from the corresponding rigid ones. Lack of residual oscillations after the completion of the useful motion at both the task and the joint-level implies good damping of the elastic modes.

Figure 5 shows the deflections at the outboard end of each one of the two flexible links. It is obvious that the strain energy residing within the flexible members is almost completely dissipated by the time the arm reaches its target position. For our adaptive demonstration, the maximum tip deflections occurring during the motion will be approximately 20 mm for the first and 8 mm for the second flexible link.

7.4. Adaptive Scheme

For our adaptive example, 10 parameters with contributions from both the robot and the manipulated payload were updated on-line, i.e., $\boldsymbol{\alpha} = [m_2, m_3,$
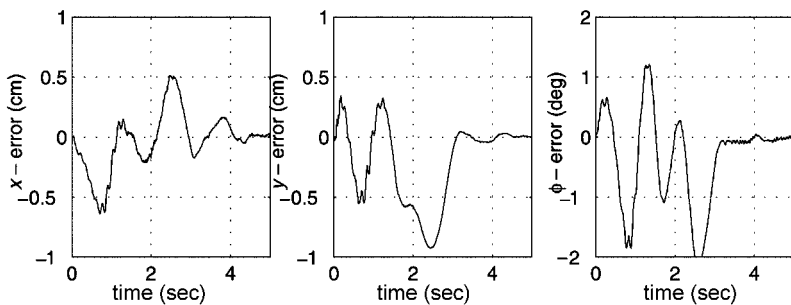
Figure 3. Tracking errors for the rigid inverse dynamics and passive feedback scheme.
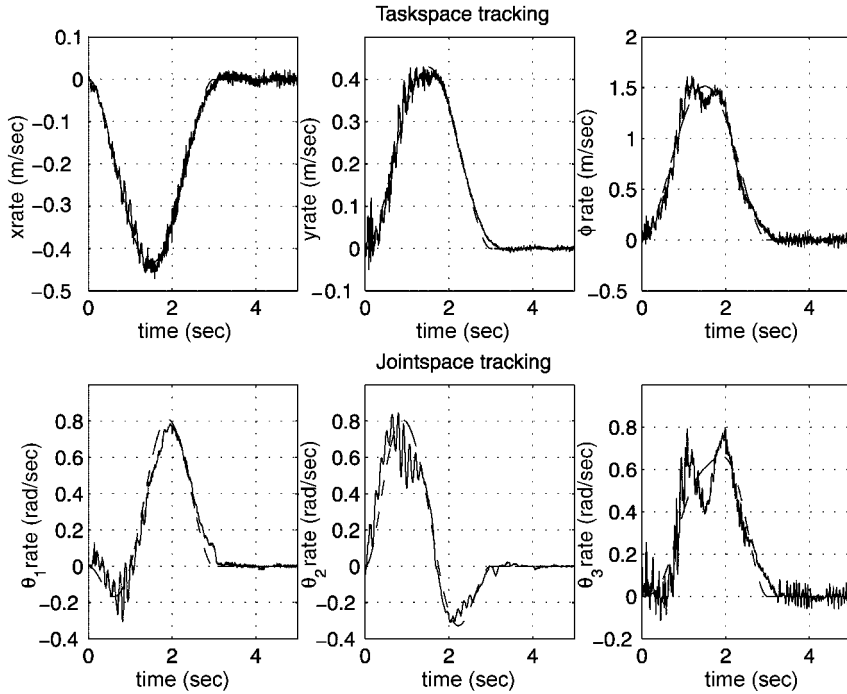
Figure 4. Rate tracking for the rigid inverse dynamics and passive feedback scheme (dashed line, desired–rigid, solid line, actual).
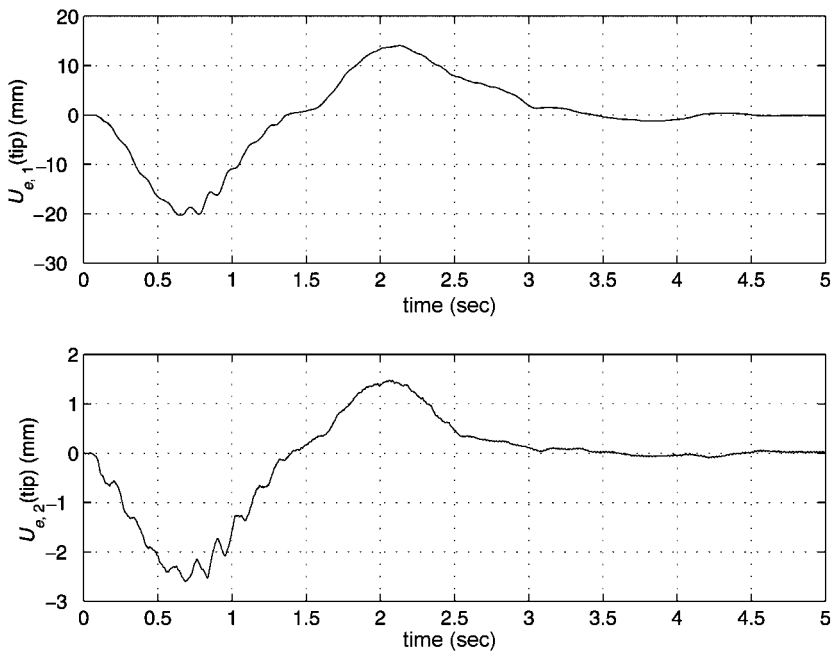
Figure 5. Deflections at the outboard end of each flexible link.
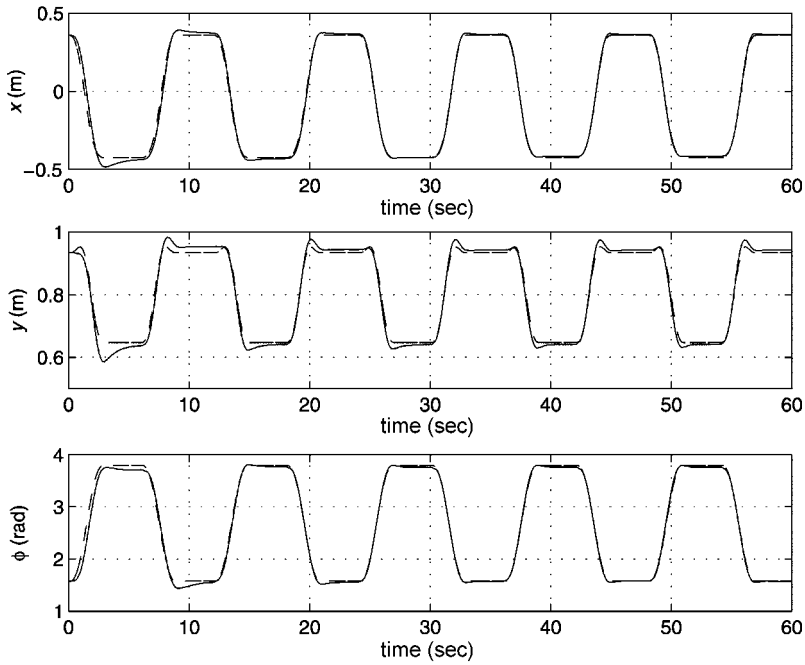
Figure 6. Task-space tracking for the adaptive scheme (dashed line, desired, solid line, actual).

$I_1, I_2, I_3, c_{x2}, c_{x3}, I_{r1}, I_{r2}, I_{r3}]^T$ where m_i is the mass, c_{xi} is the first moment of inertia along the length, and I_i is the second moment of inertia about the vertical axis of the ith link of the corresponding three-link rigid robot. Parameter I_{ri} is the inertia of rotor i, which is lumped with the corresponding joint DOF. In a realistic manipulation situation, it is more likely that the uncertainty is only with respect
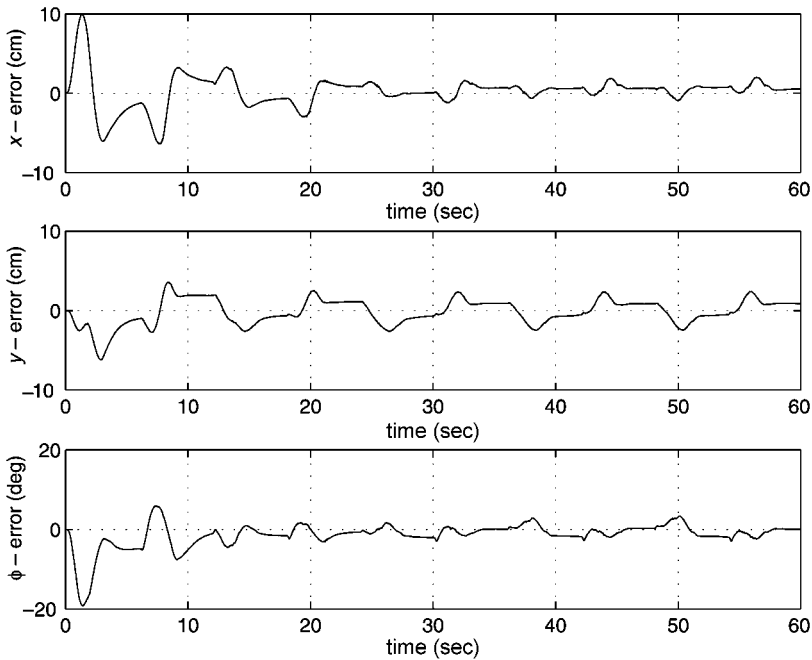
Figure 7. Tracking errors for the adaptive scheme.

to the parameters of the manipulated payload and only a few of the above parameters need to be updated on-line.

The feedback gain matrix was selected to be diagonal $K_d = \text{diag}\{22.7 \text{ N/m s}^{-1}, 35.2 \text{ N/m s}^{-1}, 0.97 \text{ N} - \text{m/rad s}^{-1}\}$, and the weighting matrix $\Lambda = I \text{ s}^{-1}$. The adaptation gains matrix was taken to be diagonal, $\Gamma = \text{diag}\{14, 10, 8, 0.7, 0.05, 15, 1, 8, 7, 2\}$, and the size of each element was manually tuned. Their relative size is related to the PE condition for the desired trajectory, which means that parameters difficult to identify require that the corresponding element in the adaptation gains matrix is large.

Figure 6 shows the task-space tracking for the three controlled task-space DOF and a value of $\mu = 0.92$. The corresponding tracking errors are given in Figure 7. Comparing each subsequent cycle, it becomes evident how performance improves with time due to adaptation. All parameters in $\boldsymbol{\alpha}$ were considered to be completely unknown and their initial estimates were set to zero. Figure 8 shows the time histories for the updated parameters, all of which are convergent. When the converged values from a previous experiment were used as initial estimates for the adaptation, the performance was much improved at the initial stages
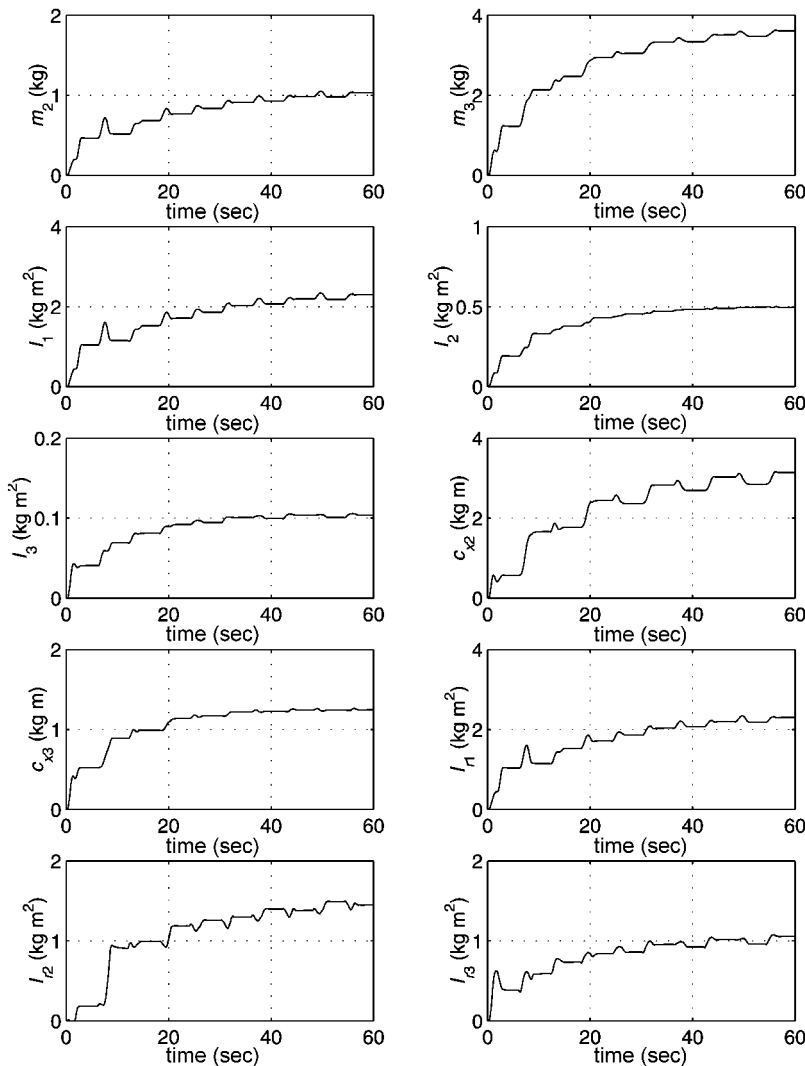
Figure 8. Parameter estimates for the adaptive scheme.
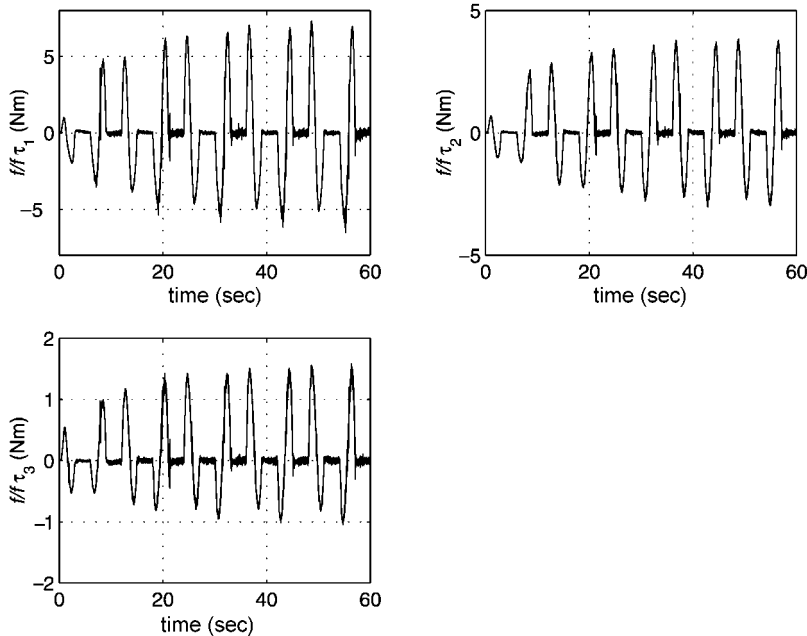
Figure 9. Adaptively updated feedforward part of the torques.

of the maneuver and the parameter estimates remained close to their initial values. Increasing the adaptation gains was found to significantly reduce the learning time and improve the tracking performance.

Figure 9 shows the adaptively updated feedforward part of the torques. At the beginning their values are zero given that we considered zero initial parameter estimates. During the learning time they increase in magnitude until they reach their steady-state values and the feedforward torques dominate the feedback ones.

8. DISCUSSION AND CONCLUSIONS

A control scheme and its adaptive version were presented which are suitable for controlling flexible-link robots carrying large payloads. Their tracking and vibration-suppression capabilities were demonstrated by experimental results. Both schemes belong to the family of passivity-based controllers which in general are claimed to exhibit good robustness characteristics. Contrary to the class of linearizing schemes they do not rely on the exact cancellation of the nonlinear effects, and the passivity theorem underlying their design yields a ''strong'' form of stability. Their robust nature was verified

by numerous tests which were not presented here due to space limitations. The tests have shown that both controllers are able to maintain stability and a good level of performance for a whole range of different payloads and maneuvers. The adaptive version was found to be effective in maintaining consistent performance in the presence of payload parameter uncertainty.

Future work will involve further study of various theoretical and implementation issues. The extension to the closed-loop configuration which represents the case of two cooperating flexible arms manipulating the same large payload will be reported elsewhere.[28]

REFERENCES

1. S.B. Skaar and C.F. Ruoff (Editors), ''Teleoperation and robotics in space,'' Progress in Astronautics and Aeronautics, Vol. 161, AIAA, Washington, DC, 1994.
2. M. Vidyasagar, System theory and robotics, IEEE Contr Syst Mag 7 (1987), 16–17.
3. R.H. Cannon Jr. and E. Schmitz, Initial experiments on the end-point control of a flexible one-link robot, Int J Robot Res 3 (1984), 325–338.
4. C.M. Oakley and R.H. Cannon Jr., End-point control of a two-link manipulator with a very flexible forearm: issues and experiments, Proc of American Control Conf, Pittsburgh, PA, 1989, pp. 1381–1396.

5. J. Carusone, K.S. Buchan, and G.M.T. D'Eleuterio, Experiments in end-effector tracking control for structurally flexible space manipulators, IEEE Trans Robot Autom 9 (1993), 553−560.

6. M.E. Demeo, M.G. Gilbert, M.A. Scott, J.A. Lepanto, E.M. Bains, and M.C. Jensen, Human-in-the-loop evaluation of remote manipulator system active damping augmentation, J. Guidance Contr Dynamics 18 (1995), 689−695.

7. M.E. Demeo, M.G. Gilbert, J.A. Lepanto, K.W. Flueckiger, E.M. Bains, and M.C. Jensen, Real-time RMS active damping augmentation: heavy and very light payload evaluations, Proc of AIAA Guidance, Navigation and Control Conf, Scottsdale, AZ, 1994, pp. 478−488.

8. E. Bayo, P. Papadopoulos, J. Stubbe, and M.A. Serna, Inverse dynamics and kinematics of multilink elastic robots: an iterative frequency domain approach, Int J Robot Res 8 (1989), 49−62.

9. B. Paden, D. Chen, R. Ledesma, and E. Bayo, Exponentially stable tracking control for multijoint flexible-link manipulators, J Dynamic Syst Meas Contr 115 (1993), 53−59.

10. S. Yurkovich and A.P. Tzes, Experiments in identification and control of flexible-link manipulators, IEEE Contr Syst Mag 10 (1990), 41−47.

11. D. Wang and M. Vidyasagar, Transfer functions for a single flexible link, Int J Robot Res 10 (1991), 540−549.

12. D. Wang and M. Vidyasagar, Passive control of a stiff flexible link, Int J Robot Res 11 (1992), 572−578.

13. H.R. Pota and M. Vidyasagar, Passivity of flexible beam transfer functions with modified outputs, Proc IEEE Int Conf Robotics Automat, Sacramento, CA, 1991, pp. 2826−2831.

14. C.J. Damaren, Passivity analysis for flexible multilink space manipulators, J Guidance Contr Dynamics 18 (1995), 272−279.

15. R. Ortega and M.W. Spong, Adaptive motion control of rigid robots: a tutorial, Automatica 25 (1989), 877−888.

16. R. Ortega, A. Loría, P.J. Nicklasson, and H. Sira-Ramírez, Passivity-based control of Euler−Lagrange systems, Springer-Verlag, London, 1998.

17. C.A. Desoer and M. Vidyasagar, Feedback systems: input−output properties, Academic Press, New York, 1975.

18. C.J. Damaren, Approximate inverse dynamics and passive feedback for flexible manipulators with large payloads, IEEE Trans Robot Automat 12 (1996), 131−138.

19. C.J. Damaren, Adaptive control of flexible manipulators carrying large uncertain payloads, J Robot Syst 13 (1996), 219−228.

20. C.J. Damaren, Modal properties and control system design for two-link flexible manipulators, Int J Robot Res 17 (1998), 667−678.

21. B. Siciliano and W.J. Book, A singular perturbation approach to control of lightweight flexible manipulators, Int J Robot Res 7 (1988), 79−90.

22. C. Canudas de Wit, B. Siciliano, and G. Bastin (Editors), Theory of robot control, Springer-Verlag, London, 1996.

23. J.-J.E. Slotine and W. Li, On the adaptive control of robot manipulators, Int J Robot Res 6 (1987), 49−59.

24. J.-J.E. Slotine and W. Li, Adaptive manipulator control: A case study, IEEE Trans Automat Contr 33 (1988), 995−1003.

25. T.I. Fossen, Comments on ''Hamiltonian adaptive control of spacecraft,'' IEEE Trans Automat Contr 38 (1993), 671−673.

26. G.G. Hastings and W.J. Book, Experiments in optimal control of a flexible arm, Proc American Control Conf, Boston, MA, 1985, pp. 728−729.

27. S.J. Miller and J.-C. Piedboeuf, Estimation of end-point position and orientation of a flexible link using strain gauges, Proc Knowledge-Based Systems and Robotics Workshop, Ottawa, Canada, 1993, p. 397−403.

28. C.J. Damaren, On the dynamics and control of flexible multibody systems with closed loops, Int J Robot Res 19, to appear.